Astron. Astrophys. 346, L37–L40 (1999)

ASTRONOMY AND ASTROPHYSICS

LETTER

Letter to the Editor

Mixing and nucleosynthesis in rotating TP-AGB stars

N. Langer[1], A. Heger[2], S. Wellstein[1], and F. Herwig[1]

[1] Institut für Physik, Universität Potsdam, Am Neuen Palais 10, D-14415 Potsdam, Germany
[2] Astronomy and Astrophysics Department, University of California, Santa Cruz, CA 95064, USA

Received 19 April 1999 / Accepted 6 May 1999

Abstract. We present the first evolutionary models of intermediate mass stars up to their thermal pulses which include effects of rotation on the stellar structure as well as rotationally induced mixing of chemical species and angular momentum. We find a significant angular momentum transport from the core to the hydrogen-rich envelope and obtain a white dwarf rotation rate comparable to current observational upper limits of $\lesssim 50\ \mathrm{km\,s^{-1}}$.

Large angular momentum gradients at the bottom of the convective envelope and the tip of the pulse driven convective shell are shown to produce marked chemical mixing between the proton-rich and the ^{12}C-rich layers during the so called third dredge-up. This leads to a subsequent production of ^{13}C which is followed by neutron production through $^{13}\mathrm{C}(\alpha,\mathrm{n})$ in radiative layers in between thermal pulses. Although uncertainties in the efficiency of rotational mixing processes persist, we conclude that rotation is capable of producing a ^{13}C-rich layer as required for the occurrence of the s-process in TP-AGB stars.

Key words: stars: evolution – stars: abundances – stars: AGB and post-AGB – stars: rotation

1. Introduction

It is known since long that thermally pulsing Asymptotic Giant Branch (TP-AGB) stars provide a site for the so called s-process, i.e., the slow neutron capture process which forms neutron-rich isotopes heavier than iron (Clayton 1968). Heavy elements primarily produced by the s-process are overabundant at the surface of AGB stars (Smith & Lambert 1990), including technetium (Little et al. 1987) which has no stable isotope and which is produced as ^{99}Tc ($\tau_{1/2} = 2.1 \times 10^5$ yr) in the s-process. In particular the roughly solar magnesium isotopic pattern found in s-process enriched AGB stars has demonstrated that the $^{13}\mathrm{C}(\alpha,\mathrm{n})$ rather than the $^{22}\mathrm{Ne}(\alpha,\mathrm{n})$ neutron source is likely to operate the s-process in AGB stars (Guélin et al. 1995, Lambert et al. 1995).

Send offprint requests to: N. Langer
(ntl@astro.physik.uni-potsdam.de)

Evidence for *in situ* s-processing is found exclusively in carbon stars (Smith & Lambert 1990), which correspond to a late evolutionary stage on the TP-AGB where the stars have large ^{12}C enrichments in their envelopes (Iben & Renzini 1983, Wallerstein & Knapp 1998). The ^{12}C enrichment implies that these stars contain, at certain times, a region at the bottom of their hydrogen-rich envelope where ^{12}C is abundant. This region where protons and ^{12}C coexist may then perhaps form ^{13}C through $^{12}\mathrm{C(p},\gamma)^{13}\mathrm{N}(\beta^+\nu)^{13}$C. Although this scenario is unrivaled, the formation of a layer which is rich in protons *and* ^{12}C in TP-AGB models has proven to be difficult, and its existence had hitherto to be assumed *ad hoc* in all s-process calculations (Gallino et al. 1998). Iben & Renzini (1982) found a ^{13}C layer in low metalicity ABG models. Recently, Herwig et al. (1997) have obtained a ^{13}C-rich layer in TP-AGB models of solar metallicity, by invoking a diffusive overshoot layer at convective boundaries. Here, we investigate for the first time effects of rotationally induced mixing processes on the TP-AGB.

2. Numerical method and physical assumptions

Our calculations have been performed with a hydrodynamic stellar evolution code (cf., Langer 1998, and references therein), which has been upgraded to include angular momentum, the effect of the centrifugal force on the stellar structure, and rotationally induced transport of angular momentum and chemical species due to Eddington-Sweet circulations, the Solberg-Høiland and Goldreich-Schubert-Fricke instability, and the dynamical and secular shear instability. We apply the rotational physics exactly as in Heger et al. (1999). In particular, the effects of gradients of the mean molecular weight μ, which pose barriers to any mixing process, have been included as in Heger et al. (i.e., $f_\mu = 0.05$). As in Heger et al., we have also included the effects of μ-barriers on convection by using the Ledoux-criterion for convection and semiconvection according to Langer et al. (1983), which is consistent with our treatment of the rotational mixing (Maeder 1997).

Changes of the chemical composition and the nuclear energy generation rate are computed using nuclear networks for the three pp-chains, the four CNO-cycles, and the NeNa- and the MgAl-cycle. Further, the 3α-reaction is included, and (α,γ)-

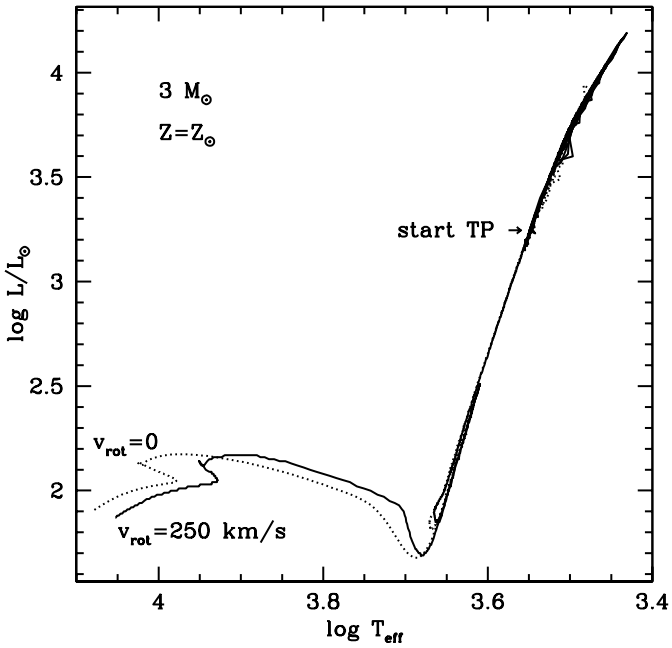

Fig. 1. Evolutionary track of our rotating $3\,M_\odot$ model (solid line) and of a non-rotating reference model (dotted line) in the HR diagram. The tracks start at the zero age main sequence and end on the TP-AGB. The beginning of the thermal pulses is marked.

reactions on ^{12}C, ^{14,15}N, ^{16,18}O, ^{19}F, ^{20,21,22}Ne, ^{24,25,26}Mg, and (α,n)-reactions on ^{13}C, ^{17}O, ^{21,22}Ne, ^{25,26}Mg. The inclusion of (n,γ)-reactions on ^{12}C, ^{20,21}Ne, ^{24,25}Mg, ^{28,29}Si allows an order of magnitude estimate of the neutron concentration. For more details see Heger et al. (1999) and Heger (1998).

3. Results

3.1. Evolution towards the TP-AGB

For our pilot study, we chose to compute the evolution of a $3\,M_\odot$ star of roughly solar composition with an initial equatorial rotation velocity of $250\,\mathrm{km\,s^{-1}}$, which is typical for late B main sequence stars (Fukuda 1982). This choice renders effects of magnetic braking and the core helium flash unimportant. The evolution of our model in the HR diagram, together with that of a non-rotating reference model, is shown in Fig. 1.

As in massive stars (Heger et al. 1999), the dominant rotational mixing process on the main sequence is the Eddington-Sweet circulation. It leads to a ^{12}C/^{13}C-ratio after the first dredge-up of 9.4, compared to a value of 19.4 in our non-rotating model (cf., Boothroyd & Sackmann 1999).

Fig. 2 sketches the evolution of the angular momentum distribution in the innermost $0.8\,M_\odot$ of our rotating $3\,M_\odot$ model. It shows that the core specific angular momentum decreases continuously during the evolution. We can give a first quantitative prediction of a white dwarf rotation rate: $\log(j/\mathrm{cm^2 s^{-1}}) = 15.3$ and $R_{\rm WD} = 0.01\,R_\odot$ yields $v_{\rm rot} = 28\,\mathrm{km\,s^{-1}}$. This is of the same order as current observational upper limits (Heber et al. 1997, Koester et al. 1998).

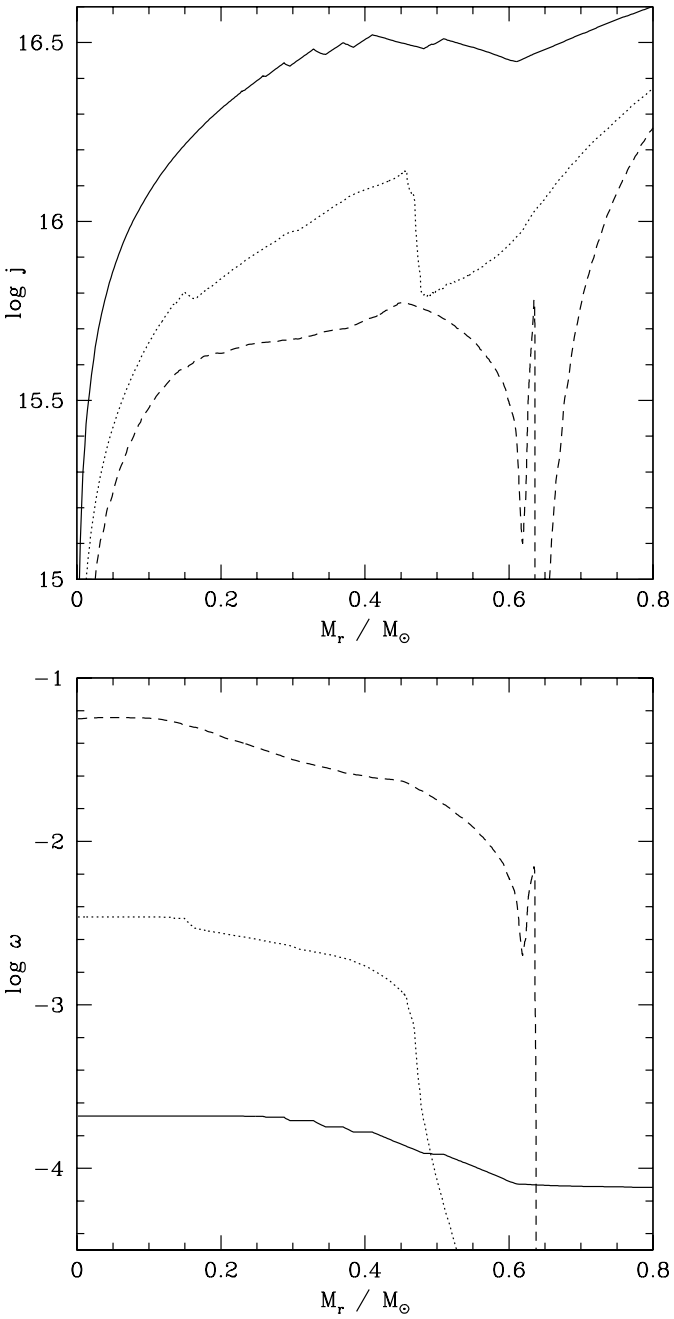

Fig. 2. *Upper panel:* logarithm of the local specific angular momentum (in $\mathrm{cm^2\ s^{-1}}$) as function of the mass coordinate for three models of our rotating $3\,M_\odot$ sequence; at core hydrogen exhaustion ($t \simeq 3.3\times10^8$ yr, solid line), during core helium burning ($t \simeq 3.8\times10^8$ yr, dotted line), and between the 14th and the 15th thermal pulse ($t \simeq 4.4\times10^8$ yr, dashed line). *Lower panel:* logarithm of the local angular velocity (in rad/s) as function of the mass coordinate for the same models which are displayed in the upper panel.

3.2. Mixing and nucleosynthesis on the TP-AGB

Fig. 3 shows the evolution of the internal structure during and after the 25th thermal pulse of our rotating model. It shows that the tip of the pulse-driven convection zone leaves after its decay a region of strong rotational mixing. This mixing be-

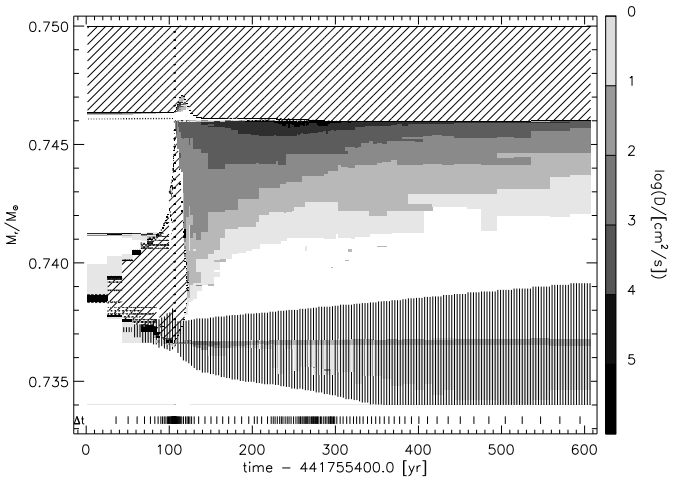

Fig. 3. Section of the internal structure during and after the 25th thermal pulse of our rotating $3\,\mathrm{M}_\odot$ sequence. Diagonal hatching denotes convection. The convective envelope extends down to $M_\mathrm{r} \simeq 0.746\,\mathrm{M}_\odot$. The pulse driven convective shell is located at $0.737\,\mathrm{M}_\odot \lesssim M_\mathrm{r} \lesssim 0.746\,\mathrm{M}_\odot$ and $30\,\mathrm{yr} \lesssim t \lesssim 120\,\mathrm{yr}$. Vertical hatching denotes regions of significant nuclear energy generation, i.e., the hydrogen burning shell (at $M_\mathrm{r} \simeq 0.746$ and $t \lesssim 100\,\mathrm{yr}$) and the helium burning shell ($0.734\,\mathrm{M}_\odot \lesssim M_\mathrm{r} \lesssim 0.739\,\mathrm{M}_\odot$ and $t \gtrsim 40\,\mathrm{yr}$). Gray shading marks regions of significant rotationally induced mixing (see scale on the right side of the figure). Vertical marks at the bottom of the figure denote the time resolution of the calculation, where every fifth time step is indicated. Cf. also Fig. 4. During this thermal pulse, the maximum energy generation rate of the helium burning shell was $4 \times 10^7\,\mathrm{L}_\odot$.

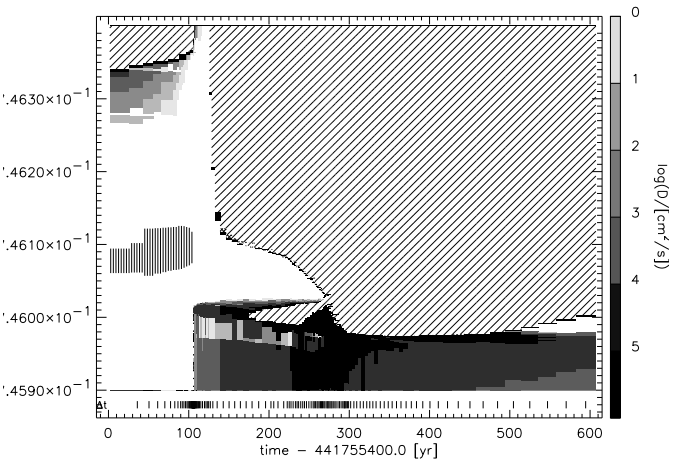

Fig. 4. Same as Fig. 3, for the same time interval, but magnifying the dredge-up of the convective envelope. Note the hydrogen burning shell source at $M_\mathrm{r} \simeq 0.7461$ and $t \lesssim 100\,\mathrm{yr}$, and the extension of the pulse driven convection zone up to $M_\mathrm{r} \simeq 0.74602\,\mathrm{M}_\odot$ at $t \simeq 100\,\mathrm{yr}$.

comes even stronger when the convective envelope extends downward during the third dredge-up event (cf. also Fig. 4). The reason is that convection enforces close-to-rigid rotation (cf. Heger et al. 1999), with an envelope rotation rate which is many orders of magnitude smaller than that of the core. The resulting strongly differential rotation (cf. also Fig. 2) allows the Goldreich-Schubert-Fricke instability, and to a lesser extent the

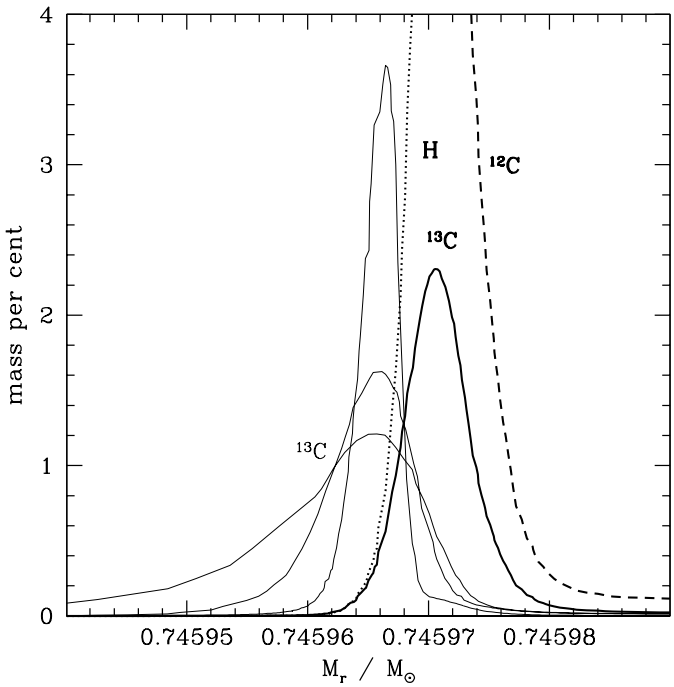

Fig. 5. Chemical profiles at the location of the maximum depth of the convective envelope during the 25th thermal pulse (cf. Fig. 4) of our rotating $3\,\mathrm{M}_\odot$ sequence. The dotted and dashed lines mark the hydrogen and the ^{12}C mass fractions at $t = 1704\,\mathrm{yr}$, with $t = 0$ defined as in Figs. 3 and 4. The fat solid line denotes the ^{13}C mass fraction at the same time. The three thin solid lines represent the ^{13}C mass fractions at $t = 2016\,\mathrm{yr}$, $t = 4155\,\mathrm{yr}$, and $t = 5139\,\mathrm{yr}$, with a later time corresponding to a smaller peak abundance. The maximum ^{13}C mass fractions of 3.6% occurs at $t = 2016\,\mathrm{yr}$. The ^{13}C peak moved inwards in the time interval from $t = 1704\,\mathrm{yr}$ to $t = 2016\,\mathrm{yr}$ due to continued proton captures on both, ^{12}C and ^{13}C.

shear instability and Eddington-Sweet circulations, to produce a considerable amount of mixing between the carbon-rich layer and the hydrogen envelope.

Fig. 5 depicts the resulting hydrogen and ^{12}C abundance profiles after the convective envelope has receded. It shows a layer of several $10^{-5}\,\mathrm{M}_\odot$ containing a large mass fraction of protons and ^{12}C at the same time. Several 1000 yr after the pulse, this layer heats up and ^{13}C is formed through proton capture on ^{12}C. Fig. 5 shows the resulting ^{13}C profiles for four different times. A maximum ^{13}C mass fraction of almost 4% is achieved.

Starting some 10^4 yr after the pulse, the ^{13}C-rich layer becomes hot enough for α-captures on ^{13}C to occur (Straniero et al. 1995). Fig. 6 shows the resulting neutron densities n_n for three different times. Note that we did not include the reaction ^{14}N(n,p)^{14}C in our network. Although most of the resulting protons may form new ^{13}C, it may be an effective neutron sink (Jorissen & Arnould 1989), in particular as also a large abundance of (primary) ^{14}N is produced in the ^{13}C-rich layer. Thus, our neutron densities can only be considered as an order of magnitude estimate. With $n_\mathrm{n} \simeq 10^7\,\mathrm{cm}^{-3}$ for $\sim 10^4\,\mathrm{yr}$, we obtain a neutron irradiation of $\tau \simeq 10^{27}\,\mathrm{neutrons/cm}^2$ which

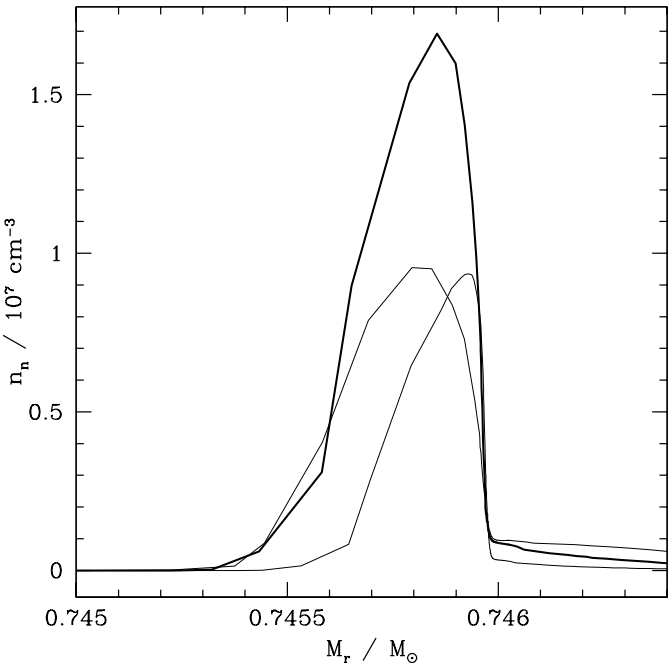

Fig. 6. Neutron density as function of the mass coordinate for three models of our rotating $3\,M_\odot$ sequence after the 25th pulse. The fat solid line corresponds to $t = 14\,150$ yr, the other two (thin solid lines) to $t = 11\,457$ yr (peak at largest mass coordinate) and $t = 16\,727$ yr, with $t = 0$ defined as in Figs. 3, 4 and 5. The time span between the 25th and the 26th thermal pulse is $\sim 30\,000$ yr.

results roughly in a number of neutron captures per iron seed of $n_c \simeq 75$, i.e. a main component s-process (cf. Figs. 7.22 and 7.23 of Clayton, 1968).

4. Discussion

By applying the concept of rotationally induced mixing as it has been developed for massive stars in our group during the last years without alteration to a $3\,M_\odot$ TP-AGB model sequence, we obtain conditions which appear favorable for the development of the s-process, i.e. a ^{13}C-rich layer which produces a considerable neutron flux later-on. Although our model develops only a very late and weak third dredge-up we believe that the mechanism which diffuses the protons into the carbon layer and ^{12}C into the envelope must occur with a similar magnitude in all TP-AGB stars which develop a third dredge-up. The reason is that the huge specific angular momentum jump at the hydrogen/carbon interface — five orders of magnitude in our case — is independent of the depth of the third dredge-up.

The maximum ^{13}C abundance and its distribution in our model is, at first, similar to that found due to diffusive convective overshooting by Herwig et al. (1997). However, in our case the rotational mixing spreads the ^{13}C peak out before the neutrons are produced (cf. Figs. 5 and 6), which is not the case in the models of Herwig et al. (1997). At the present time we can not discriminate which of these scenarios would agree better with empirical constraints. However, we want to stress that both mechanisms of ^{13}C production, rotation and overshooting, do not exclude each other, and that it is possible that they act simultaneously in AGB stars.

Finally, we want to emphasize that, although stars of less than $\sim 1.3\,M_\odot$ lose 99% of their angular momentum due to a magnetic wind during their main sequence evolution, it can not be excluded that the proposed mechanism of ^{13}C-production due to differential rotation also works for them. Certainly, the sun's core will spin-up and the envelope will further spin down during its post-main sequence evolution, which may result in a specific angular momentum jump of similar magnitude. The investigation of the mass and metallicity dependence of the production of ^{13}C due to rotation is an exciting task for the near future.

Acknowledgements. We are grateful to Thomas Blöcker for many fruitful discussions. This work has been supported by the Deutsche Forschungsgemeinschaft through grants La 587/15-1 and 16-1.

References

Boothroyd A.I., Sackmann I.-J., 1999, ApJ 510, 232
Clayton D.D., *Principles of stellar evolution and nucleosynthesis*, University of Chicago Press, Chicago
Fukuda I., 1982, PASP 94, 271
Gallino R., Arlandini C., Busso M., Lugarno M., Travaglio C., Straniero O., Chieffi A., Limongi M., 1998, ApJ 497, 388
Guélin M., Forestini M., Valiron P., Anderson M.A., Cernicharo J., Kahane C., 1995, A&A 297, 183
Heber U., Napiwotzki R., Reid I.N., 1997, A&A 323, 819
Heger A., 1998, PhD thesis, TU München (MPA green report No. 1120)
Heger A., Langer N., Woosley S.E., 1999, ApJ, submitted (astro-ph/9904132)
Herwig F., Blöcker T., Schönberner D., El Eid M.F., 1997, A&A 324, L81
Iben I. Jr., Renzini A., 1982, ApJ 263, L23
Iben I. Jr., Renzini A., 1983, ARAA 21, 271
Jorissen A., Arnould M., 1989, A&A 271, 161
Koester D., Dreizler S., Weidemann V., Allard N.F., 1998, A&A 338, 617
Lambert D.L., Smith V.V., Busso M., Gallino R., Straniero O., 1995, ApJ 450, 302
Langer N., 1998, A&A 329, 551
Langer N., Fricke K.J., Sugimoto D., 1983, A&A 126, 207
Little S.J., Little-Marenin I.R., Hagen Bauer W., 1987, AJ 94, 981
Maeder A., 1997, A&A 321, 134
Smith V.V., Lambert D.L., 1990, ApJS 72, 387
Straniero O., Gallino R., Busso M., Chieffi A., Raitieri C.M., Solaris M., Limongi M., 1995, ApJ 440, L85
Wallerstein G., Knapp G.R., 1998, ARAA 36, 369